Available online at www.sciencedirect.com
ScienceDirect
Journal of Nuclear Materials 374 (2008) 354–363
journal of nuclear materials
www.elsevier.com/locate/jnucmat

Creep behavior of niobium-modified zirconium alloys

I. Charit *, K.L. Murty [1]

North Carolina State University, Nuclear Engineering Department, 2113 Burlington Engineering Laboratories, 2500 Stinson Drive, Raleigh, NC 27695, USA

Received 20 February 2007; accepted 28 August 2007

Abstract

Zirconium (Zr) alloys remain as the main cladding materials in most water reactors. Historically, a series of Zircaloys were developed, and two versions, Zircaloy-2 and -4, are still employed in many reactors. The recent trend is to use the Nb-modified zirconium alloys as the Nb addition improves cladding performance in various ways, most significant being superior long term corrosion resistance. Hence, new alloys with Nb additions have recently been developed, such as Zirlo™[2] and M5™[3]. Although it is known that creep properties improve, there have been very few data available to precisely evaluate the creep characteristics of new commercial alloys. However, the creep behavior of many Nb-modified zirconium alloys has been studied in several occasions. In this study, we have collected the creep data of these Nb-modified alloys from the open literature as well as our own study over a wide range of stresses and temperatures. The data have been compared with those of conventional Zr and Zircaloys to determine the exact role Nb plays. It has been argued that Nb-modified zirconium alloys would behave as Class-A alloys (stress exponent of 3) with the Nb atoms forming solute atmospheres around dislocations and thus, impeding dislocation glide under suitable conditions. On the other hand, zirconium and Zircaloys behave as Class-M alloys with a stress exponent of $\geqslant 4$, attesting to the dislocation climb-controlled deformation mode.

1. Introduction

Zr alloys are used extensively as the fuel cladding tubes for encapsulating fuel pellets, and for other structural applications in light water reactors (LWR). For instance, recrystallized Zircaloy-2 is used in boiling water reactors (BWR) and cold-work-stress-relieved (CWSR) Zircaloy-4 in pressurized water reactors (PWR). Zircaloys are Zr alloys containing Sn, Fe and Cr as alloying elements. In pressurized heavy water reactors (PHWR), Zr–2.5 wt% Nb alloy is used as pressure tubes. The safety and reliability of a reactor largely depend on the cladding performance. The cladding tube is subjected to various thermal and multiaxial stress conditions inside the reactor [1]. A typical PWR core may experience temperatures in the range of 290–350 °C and a system pressure of 15–16 MPa during normal operation [2,3]. In addition, stresses arise from the external pressure of the coolant, flow-induced vibration, internal pressure due to released fission gases, pellet cladding mechanical interaction and spacer grid forces due to differential growth leading to fuel rod bow. Hence an understanding of the high temperature deformation behavior of the cladding materials in a wide range of stresses and temperatures is essential to make mitigating plans in the event of an untoward incident (such as, loss-of-coolant accident or LOCA). Creep behavior of Zr and its alloys has been investigated over many decades, and been reviewed [4,5]. The history of the Zircaloy development has been quite interesting [6,7]. By 1965, Zircaloys became the main cladding material in almost all the LWRs operating in the West. In the erstwhile USSR, Ozhenite alloys which are complex Zr-base alloys with a total amount of Sn, Fe, Ni, Nb etc. alloying elements in the range of

* Corresponding author. Present address: University of Idaho, Moscow, ID 83844-3024, USA. Tel.: +1 208 885 5964; fax: +1 208 885 0154.
E-mail addresses: icharit@uidaho.edu (I. Charit), murty@ncsu.edu (K.L. Murty).
[1] Tel.: +1 919 515 3657; fax: +1 919 515 5115.
[2] Zirlo™ is a trademark of Westinghouse Electric Company, Pittsburgh, PA.
[3] M5™ is a trademark of Framatome ANP, Lynchburg, VA.

0022-3115/$ - see front matter © 2007 Elsevier B.V. All rights reserved.
doi:10.1016/j.jnucmat.2007.08.019

0.5–1.5 wt% were investigated for cladding applications. However, Nb-modified Zr alloys (such as E110 and E635, main composition being Zr–1 wt% Nb) were found most suitable for cladding applications in the VVER and RBMK-type Russian water reactors [8]. It was recognized that Nb addition in Zr alloys improves the long-term corrosion resistance and mechanical properties as well as retains a low neutron capture cross-section in the cladding, leading to extended fuel cycles with higher burn-ups. Following the Russian experience, Canadian researchers developed Zr–2.5Nb alloys which are used in PHWR (CANDU) reactors. Recently, several niobium-modified Zr alloys (such as, Zirlo and M5) have been developed for use in cladding applications in the USA and Europe. These are the alloys that are going to be used in modern light water reactors. Unfortunately, there is a paucity of creep data for these new Zr alloys including biaxial creep, as evident from the survey of the recent literature.

There are creep data available for the earlier developed commercial and experimental Nb-modified Zr alloys. This study aims to pull together results from those studies as well as from our own, and analyze them in the light of existing creep theories. The aim is to develop a unified mechanistic understanding of the thermal creep behavior of these materials. The data are also compared with the representative creep data of Zr and Zircaloys to bring out the significance of the Nb addition on the creep properties.

1.1. Zr–Nb system

The chemical compositions of different Zr alloys used for reactor applications are shown in Table 1. It shows the major differences in various alloy compositions.

Zr and Nb are in the IVB and VB groups of the Periodic Table, respectively. Their crystal structures at lower temperatures are different (α-Zr is hcp and Nb is bcc). However, at >865 °C Zr assumes a bcc crystal structure [3]. Nb is considered a strong β-phase stabilizer. Depending on the processing (such as, heat treatment), various types of microstructures can be produced. Hence, a full knowledge of microstructural characteristics is essential while discussing creep properties of the respective alloys. Further, it is important to note that the impurity content may also influence the solubility of Nb in Zr.

Bethune and Williams [9] noted that there had been much disagreement about the maximum solubility of Nb in α-Zr. From a literature survey, it was found to vary from 0.6 to as high as 6.4 wt%. Okamoto [10] has shown that the maximum solubility of Nb in α-Zr is ~0.6 wt%. According to the phase diagram, the solubility of Nb at <400 °C is very small, and the most Nb remains in some form of precipitates (β-Nb). Further, according to the Zr–Nb phase diagram the monotectoid reaction ($\alpha_{Zr} + \beta_{Nb} \rightarrow \alpha_{Zr} + \beta_{Zr}$) can occur at about 620 °C. However, a recent study by Canay et al. [11] revealed that the monotectoid reaction temperature for a Zr–1Nb alloy is ~776 °C and the transus temperature is ~948 °C for total transformation to β_{Zr}. Other minor impurities (such as, oxygen) also may change the transformation temperatures. Hence, the interpretation of creep data above that temperature range must take into account the consequence of phase changes. However, Zr alloys containing ~1.0 wt% Nb can be considered as a quasi-single phase alloy because the volume fraction of the Nb-containing second phases remains very small. In this paper, we have focused our discussion on the creep characteristics of Zr-based alloys containing ~1.0 wt% Nb or less.

Fig. 1 shows bright field TEM images of a recrystallized Zr–1Sn–1Nb–0.2Fe [12]. Fig. 1(a) shows the α-Zr matrix grains with a small volume fraction of β-Zr phase present only at the grain boundaries. The dislocation structures present in this as-recrystallized alloy is shown in Fig. 1(b).

1.2. Various creep mechanisms

It has been observed that diffusional processes become increasingly important at temperatures above about 0.3–0.4 T_m and high temperature deformation behavior can be described by the following equation:

$$\dot{\varepsilon} = A\frac{DEb}{kT}\left(\frac{\sigma}{E}\right)^n\left(\frac{b}{d}\right)^p, \quad (1)$$

where $\dot{\varepsilon}$ is the steady-state strain rate, σ is the applied stress, d the grain size, A is a constant dependent on the material and operating mechanism, D is the diffusivity [which is of the functional form, $D_0\exp(-Q/RT)$, where D_0 is the frequency factor, Q the appropriate activation energy, R the universal gas constant and T the temperature in K], E the elastic modulus, b the Burgers vector, k the

Table 1
Chemical composition of various Zr Alloys (in wt%) [8]

Materials	Nb	Sn	Fe	Cr	O
E110	0.95–1.05	–	0.006–0.012	–	⩽0.10
E110K	0.95–1.05	–	0.006–0.012	–	0.12–0.16
E635	0.95–1.05	1.10–1.30	0.30–0.40	–	0.05–0.12
M5	0.80–1.20	–	0.015–0.06	–	0.09–0.13
Zirlo	0.9–1.13	0.90–1.2	0.1	–	0.09–0.15
MDA	0.5	0.8	0.2	0.1	–
Zircaloy-4	–	1.20–1.70	0.1	0.07–0.13	0.09–0.13

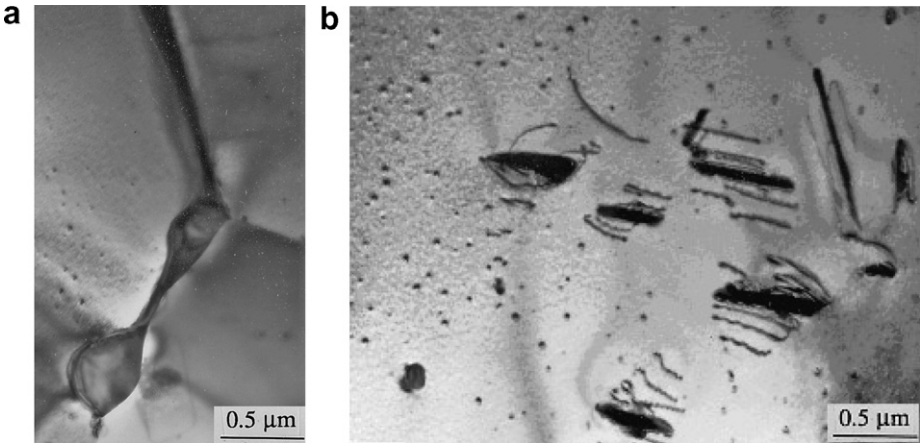

Fig. 1. (a) Recrystallized grain structure of a Zr–1Sn–1Nb–0.2Fe alloy showing α-Zr grains with β-Zr phases as boundary phases. (b) Dislocation structures in the same alloy.

Boltzmann's constant, n the stress exponent and p the inverse grain size exponent.

Detailed accounts of various creep mechanisms can be found in the literature [13–18]. The creep behavior of pure metals and some alloys is termed as the Class-M (or Class-II) type. A stress exponent of 5 is expected. However, stress exponents of 4–7 generally fit the creep behavior of a Class-M alloy. Although there are a number of models describing the Class-M behavior, Weertman's pill-box model continues to be widely accepted [17]. In this model, the dislocations generated by the Frank–Read sources keep on gliding until the edge components of the dislocations are hindered from further movement due to the mutual elastic repulsion, whereas the screw components cross-slip rapidly for mutual annihilation. At high homologous temperatures, diffusion of vacancies become rapid enough for edge dislocations to climb toward each other and in the process, mutually annihilate. Then, Frank–Read sources start operating again. The steady state is reached when the rates of recovery and work hardening become equal. This creep mechanism is grain size independent, and generally associated with a stress exponent of 4–7. At higher stresses (at $\sim 10^{-3}$ E) creep rates become higher than what is expected from the power law creep, and follow an exponential relation. This is called power law breakdown (PLB) regime. Dislocation mechanisms occurring in the PLB regime are not clearly resolved, but it is thought to be essentially the same as in the power-law regime at lower stresses.

At lower stresses, Newtonian viscous creep mechanisms ($n = 1$) are expected to operate. Depending on the grain size and/or temperature, the grain boundary or lattice diffusivity becomes dominant. At higher temperatures and small grain sizes, Nabarro–Herring (N–H) creep is dominated by the bulk diffusion. N–H creep is grain size dependent ($p = 2$). At even smaller grain sizes or lower temperatures, grain boundary diffusion becomes more significant. Then, a different diffusion creep mechanism, known as Coble creep, operates. This creep mechanism is more grain size sensitive than the N–H creep ($p = 3$). At very large grain sizes creep rate becomes grain size independent and follows Harper–Dorn creep (H–D) with an activation energy equal to that for volume diffusion.

The creep behaviors of many solid solution alloys are termed as Class-A (or Class-I) type [14–16]. Here solute atoms lock the mobile dislocations in such a way that the glide process becomes sluggish compared to the climb process under a range of creep conditions. As the climb and glide operate in sequence, the slower one i.e. the dislocation glide controls the rate. The activation energy associated with this mechanism is that of solute diffusivity in solid solution (or Darken diffusivity). However, for all practical purposes, the lattice self-diffusivity and Darken diffusivity are comparable, especially in dilute alloys. If the stress is decreased further, the dislocation climb controlled regime would appear. However, diffusional creep may still be observed at further lower stresses. On the other hand, at higher stresses dislocations may breakaway from the solute atmospheres, thus entering a climb-controlled regime again. This regime is associated with similar characteristics as the climb-controlled regime already discussed ($n = 4$–7). Following Murty's work [15,16,18], this breakaway stress can be calculated from the equation

$$\sigma_b = \frac{W_m^2 c_o}{2^\beta kTb^3}, \tag{2}$$

where W_m is the binding energy between solute atom and the dislocation, c_o is the solute concentration, and β typically ranges between 2 and 4 depending on the shape of the solute atmosphere. Later, Langdon and coworkers [14,19] showed that this relation is valid for a number of solid solution alloys. Assuming 0.23 eV as a reasonable value for W_m, the critical stress for breakaway is estimated to be $\sim 7.5 \times 10^{-4}$ E, which is in agreement with the experimental results obtained from various Class-A alloys [18].

At even higher stresses, there may appear another regime involving low temperature climb controlled creep with a stress exponent value of $n + 2$ (i.e. 7). This mechanism is associated with the climb processes involving

Table 2
Parametric dependencies of various diffusion-controlled deformation mechanisms [1,18]

Mechanism	D	n	p	A
Climb of edge dislocations	D_L	5	0	$\sim 6\times 10^7$
Viscous glide	D_S	3	0	6
Low temperature climb	D_C	7	0	2×10^8
Harper–Dorn	D_L	1	0	3×10^{-10}
Nabarro–Herring	D_L	1	2	12
Coble	D_B	1	3	100

Note. D_L: lattice diffusivity, D_S: solute diffusivity, D_C: dislocation core diffusivity, and D_B: grain boundary diffusivity.

dominance of dislocation core diffusion. However, this is often masked because the power law breakdown regime starts in the near vicinity. Table 2 presents parametric dependencies and constants for relevant deformation mechanisms.

It is important to note that a number of activation energy values for lattice self-diffusion in α-Zr have been available in the literature. There was much confusion regarding activation energy values of intrinsic self and substitutional diffusion in α-Zr, and Hood and coworkers [20–22] have treated the subject extensively. It is now known that the activation energy value in α-Zr (~300 kJ/mol) is much higher than originally thought of mainly because of the extrinsic impurity effects. For example, the presence of minor amount of iron tends to lower the diffusivity as Fe atoms appear to diffuse through Zr lattice interstitially very rapidly and form a complex with Zr vacancy. Eq. (3) determined by Lyashenko et al. [23] has been used here to evaluate the appropriate diffusivity value as it appears to be the most compatible with the experimental data under consideration. Thus, the following diffusivity [23] and temperature-dependent elastic modulus (E_T) were utilized in the normalization procedure for this study:

$$D = 1.26\times 10^{-3}\exp(-272000\ \mathrm{J}/RT)\mathrm{m}^2\ \mathrm{s}^{-1} \quad (3)$$

and

$$E_T = (88000 - 61.4T)\ \mathrm{MPa}, \quad (4)$$

where T is in K.

2. Creep characteristics of Zr–0.5Nb alloy

Pahutova et al. [24] conducted a detailed creep study on a Zr alloy containing 0.5 wt% Nb with an average grain diameter of 500 μm. They reported a stress-independent creep activation energy of 288 ± 25 kJ/mol, which is in agreement with the activation energy for lattice self-diffusivity (272 kJ/mol) [24]. All the stress and steady state strain rate data (test temperatures ranging 350–550 °C) of this alloy are plotted on a normalized basis (i.e. compensating with the appropriate diffusivities and moduli) in Fig. 2. This alloy consisted of equiaxed α-Zr phase and some lath martensite. Three deformation regimes can be recognized in Fig. 2. At the intermediate normalized stresses, a region

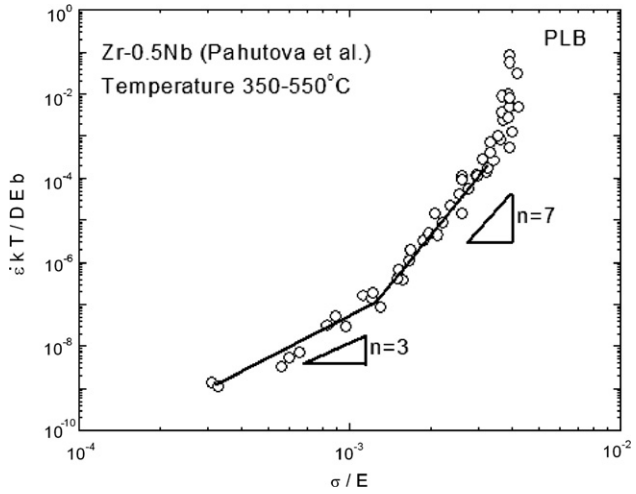

Fig. 2. Stress and strain rate data of Zr–0.5Nb alloy shown on a normalized basis [24].

with a stress exponent value of 7 was obtained. The authors attributed the deformation due to recovery occurring through dislocation annihilation by climb. Microstructural observation in this regime through transmission electron microscopy (TEM) revealed a well-developed subgrain structure as is expected in climb creep regime. Generally, high temperature climb is associated with stress exponents of 4–7. However, it is also known that a stress exponent of ~7 may be a characteristic of a low temperature dislocation-climb controlled mechanism (Table 2). It is known that this kind of mechanism would require an activation energy for dislocation core diffusion. But as already mentioned, the measured activation energy was consistent with that of the lattice self-diffusion. Also, notable is that the upper portion of these data is close to the PLB regime, and the transition from the power law dependence to an exponential dependence of stress occurs.

At lower normalized stresses, there appears a deformation regime with a stress exponent of ~3, which is controlled by the viscous glide of dislocations. The possibility of the viscous glide regime was confirmed from the substructure of the crept sample (tested at a normalized stress of $\sim 3\times 10^{-4}$) investigated by TEM. As expected, no subgrain formation was observed, and dislocations were randomly arranged in the α-Zr grains, which is characteristic of the viscous dislocation glide. Thus we note the operation of glide and climb creep mechanisms taking place in series as expected in Class-A type alloys.

3. Creep characteristics of Zr–1Nb alloy

In an earlier study by Thorpe and Smith [25], it was reported that the creep curves in Zr–1Nb alloy almost never reach the steady state. The material used in that study was recrystallized with a mean linear intercept grain size of 2.2 μm. The test temperatures varied from 100–500 °C. Dynamic strain aging was observed to influence

the deformation behavior in the vicinity of 257 °C. An attempt was made to explain the behavior with recovery and hardening effects. Although the steady-state was not achieved, the stress sensitivity of the creep rate in the transient regime (at 5% creep strain) was 8.4 at 400 °C, and 8.0 at 500 °C. However, no microstructural evidence was presented.

Alymov et al. [26] referred to a work by Voeikov et al. [27] where stress exponents of ~5 and a creep activation energy of 214 kJ/mol were obtained while investigating steady-state creep of Zr–1Nb tubes in the temperature range of 347–397 °C and a stress range of 70–120 MPa ($1.4–2.6\times10^{-3}$ E). Although from the initial study, it may appear Zr–1Nb acts like a Class-M alloy, the stress and temperature ranges investigated were too narrow to reach any definitive conclusion.

Alymov and coworkers [26,28–30] generated a vast amount of high temperature deformation data in a wide range of conditions. The work was carried out in the single phase regime of the alloy at a temperature range of 377–597 °C and a stress range of 10–150 MPa (2×10^{-4}–4×10^{-3} E) [26]. The initial microstructure of the alloy was completely recrystallized with a grain size of ~5 μm. An apparent activation energy of 240 ± 10 kJ/mol was obtained. By modulus compensation, a true activation energy of 235 ± 10 kJ/mol was derived. The activation energy was not influenced by stress or temperature ranges. However, the value of activation energy was found to be below the activation energy of 272 kJ/mol found by Lyashenko et al. [23]. Although they did not present any microstructural evidence, they suggested that the stress exponent of ~5 obtained above a stress level of 32 MPa is a direct evidence of the operation of dislocation climb-controlled mechanism. A stress exponent of 2.2 was obtained for tests conducted below a stress level of 32 MPa, which implied the operation of grain boundary sliding related mechanism. They also constructed an approximate deformation mechanism map considering that at very low stresses, Coble creep would operate, but again no direct evidence was presented. Fig. 3 shows the normalized stress and strain rate plots of the creep data. There appear only two distinct deformation regimes, one with a stress exponent close to 5 at higher σ/E values and the other with a stress exponent value of ~3 at lower modulus-compensated stresses. Hence, there appears to be a transition in deformation similar to that of Zr–0.5Nb alloy discussed earlier. However, it is not clear whether the PLB regime appears at higher stresses because of the lack of enough data.

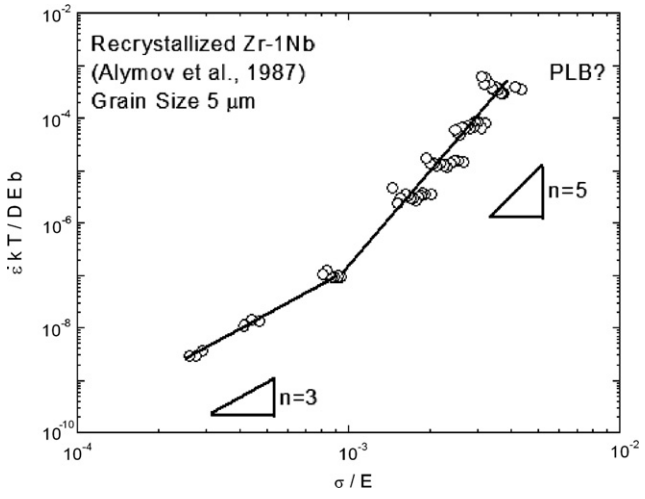

Fig. 3. The variation of strain rate as a function stress using proper modulus and diffusivity compensation [26].

In a different study, Pirogov et al. [29] reported a comparative account of the creep characteristics involving a fully recrystallized and a cold worked Zr–1Nb alloy. The former material had an average equiaxed grain size of 8 μm while the latter one had a 'fibrous' (presumably elongated) microstructure with an average 'fiber' (presumably grain) thickness of 3 μm. It was noted that the creep resistance of the cold worked alloy was significantly greater than that of the recrystallized alloy, particularly for shorter pre-test holding times. The cold worked microstructure evolved throughout the creep test, and underwent in situ recrystallization process. They noted that for these types of alloys, two characteristic creep rates may be important, a minimum creep rate, and a final creep rate that resembles the steady state creep rate of the fully recrystallized structure.

Fig. 4(a) and (b) shows the normalized creep rate versus stress data for the recrystallized and cold worked alloy, respectively. The normalization gives a poor correlation factor between various data. Also, on these plots the significant strength enhancement of the cold worked structure against the recrystallized one is not readily evident. Although there is significant scatter in the data, they do seem to indicate a stress exponent of 3 at lower stresses ($<2\times10^{-3}$ E) while a larger value of 8 (cold worked) and 6 (recrystallized) at higher stresses, again indicating the Class-A type behavior.

Pirogov et al. [30] also investigated the creep behavior of Zr–1Nb in a temperature regime of 607–877 °C. The $\alpha/\alpha+\beta$-phase boundary as per Zr–Nb phase diagram occurs at ~600 °C, and thus, the microstructure would transform into a two-phase microstructure with significant β-Zr phase present across the temperature ranges. The α-Zr phase gradually disappears with increasing temperature, and new β-Zr phases appear. The grain size also increased from <10 μm to as high as 70 μm. An equation resembling the rule of mixture was introduced to take care of the concomitant presence of α-Zr and β-Zr phases. They proposed constitutive equations at various stages of transformation. However, more detailed study is needed to elucidate the creep behavior in such a regime.

Very high temperature creep and tensile tests (897–1097 °C) of Zr–1Nb alloy were also conducted by Alymov and coworkers [28]. In this temperature range, Zr presumably remains in the β-Zr form due to higher temperatures. However, it has been found that oxygen elevates the

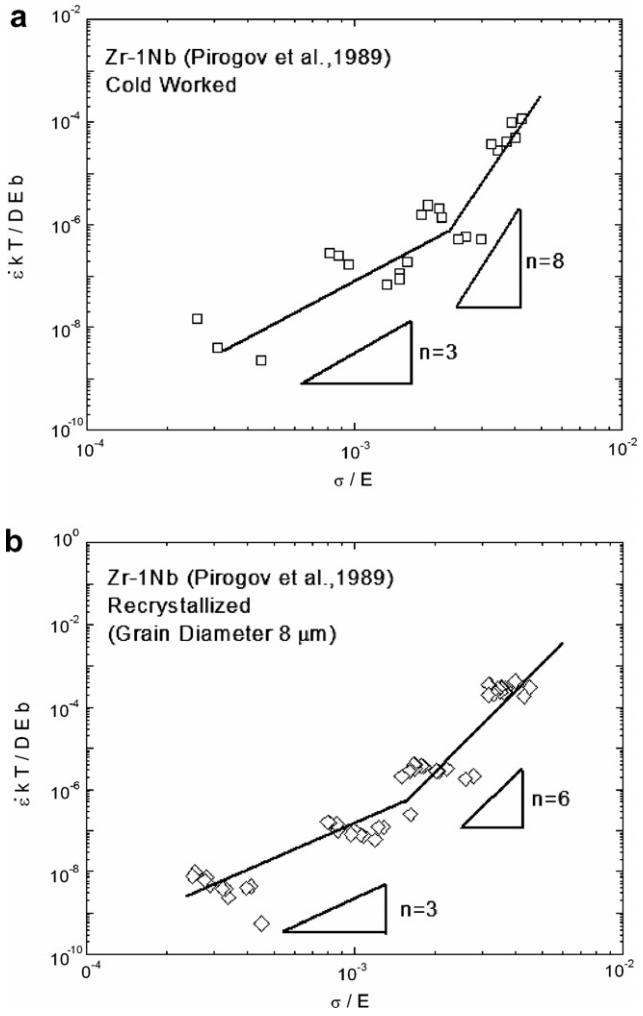

Fig. 4. Plots of normalized strain rates vs. stresses comparing the creep behavior of (a) a cold worked and (b) a recrystallized Zr–1Nb [29].

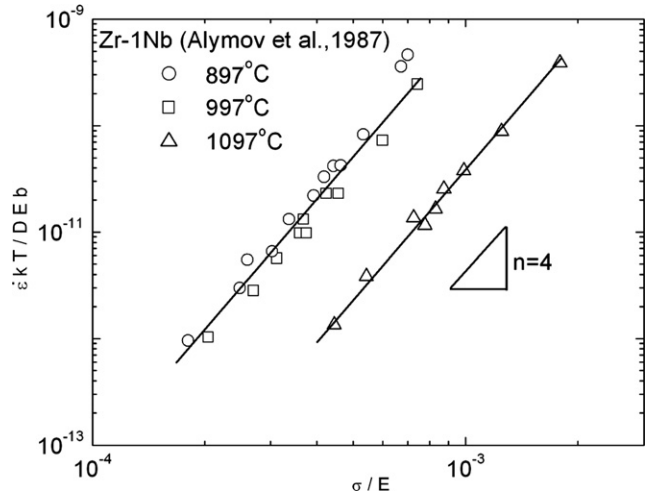

Fig. 5. Normalized strain rate vs. stress for a Zr–1Nb alloy in the temperature range of 897–1097 °C [28].

$\alpha + \beta \rightarrow \beta$ transus temperature at a rate of ~0.06 °C/wt ppm. Further, Canay et al. [11] have measured the β transus temperature for Zr–1Nb alloy to be ~948 °C. Given that the oxygen impurity was kept at a very small level and no quantitative oxygen content was reported, the relevant temperature of transformation then becomes a subject of speculation. However, Alymov et al. [28] reported an activation energy value of 110 kJ/mol, which is identical to the activation energy (~110 kJ/mol) for lattice self-diffusivity of Zr in Zr–1Nb alloy in the β-Zr phase regime [31]. Alymov et al. [28] reported an apparent stress exponent of 3.5. They argued that some deformation mechanism between the viscous glide and dislocation climb may be operating in this regime. However, with appropriate diffusivity and modulus compensation (Fig. 5), the true stress exponent was found to be 4 in our analysis. From that knowledge, it is appropriate to suggest that the deformation regime is dislocation climb controlled.

The data of two lower temperatures (897 and 997 °C) fall close to each other whereas the highest temperature data (for 1097 °C) are radically different (shifted to the right of the lower temperature data line) even though the diffusivity-compensated creep rate range remained quite similar. This leads one to believe that this difference arises because of the microstructural transformation. It is interesting to note that in the lower temperature range the microstructure may quite possibly be in the two-phase (α/β) region. Although they will have different volume fractions of α and β phases at two temperatures (897 °C and 997 °C), the use of β-Zr self-diffusivity still gives good correlation, which may not have much of a meaning. Moreover, the microstructure at the highest temperature level (1097 °C) is fully in β-Zr form beyond reasonable doubt. Then the use of β-Zr self-diffusivity for lower temperature data may not have any real meaning even though they correlate well. The reason for this behavior is not clear at this point, and due to the lack of sufficient microstructural evidence the above explanation remains more of a conjecture.

4. Creep mechanisms in Zirlo

Zirlo is basically a Nb-modified Zircaloy. Murty et al. [32,33] made tensile creep tests in both rolling (RD) and transverse (TD) directions of a Nb-modified Zircaloy (Zr–1Sn–1.0Nb–0.2Fe, by wt%) sheet. The material had a recrystallized microstructure with an average grain diameter of 8 μm. Both the RD and TD specimens show similar trends and the minor variation in strain rates was characteristic of minute planar anisotropy of the sheet. According to Canay et al. [11], the temperature of $\alpha \rightarrow \alpha + \beta$ transformation in Zr–1Nb–0.8Sn–0.2Fe alloy is 741 °C. Therefore, it can be reasonably assumed that at the highest test temperature (i.e. 650 °C), most α-Zr phases were retained without the possibility of substantial β-Zr phase formation. When steady-state strain rates were plotted as a function of stresses, they exhibited three distinct deformation regimes ($n = 1$, $n = 3$ and $n = 7$, with incrementing stress levels). In the lower stress regime, a mean activation energy

of ~126 kJ/mol was obtained, and this value corresponded to the activation energy for grain boundary diffusion in α-Zr (143.8 kJ/mol) [12]. A comparison with standard models revealed that the lower stress regime with $n = 1$ represents Coble creep, and not Nabarro–Herring or Harper–Dorn creep with similar stress dependencies consistent with the relatively small grain size (8 μm) of the experimental alloy.

The second regime at the intermediate stresses shows a stress exponent of 3, which is characteristic of viscous dislocation glide. An activation energy of ~282 kJ/mol was obtained. This value is close to the activation energy for lattice self-diffusion in α-Zr (~272 kJ/mol) identifiable with the appropriate diffusivity in a dilute solid solution.

At higher stresses (third regime), a stress exponent of ~7 was obtained. As discussed earlier, it most likely involves the operation of dislocation climb related processes with an activation energy close to that of lattice self-diffusion. At even higher stresses, the strain rate increases at a rate higher than definable by the power law, and thus, PLB starts. Fig. 6 shows a composite curve in normalized strain rates and stresses using all the creep data obtained for this material. In this figure, we use lattice self-diffusivity for compensation. As a result, the lower stress regime data (Coble creep) did not fall together. However, the other data correlate very well in the other two regimes ($n = 3$ and 7). An important observation from this figure is that at temperatures below a specific temperature, the viscous glide regime disappears, and dislocation climb controlled regime appears with a direct transition from diffusional creep. The equations defining the two dislocation creep regimes are

$$\dot{\varepsilon} = 4.4\frac{DEb}{kT}\left(\frac{\sigma}{E}\right)^3, \tag{5}$$

and

$$\dot{\varepsilon} = 2\times 10^{11}\frac{DEb}{kT}\left(\frac{\sigma}{E}\right)^7, \tag{6}$$

respectively [30].

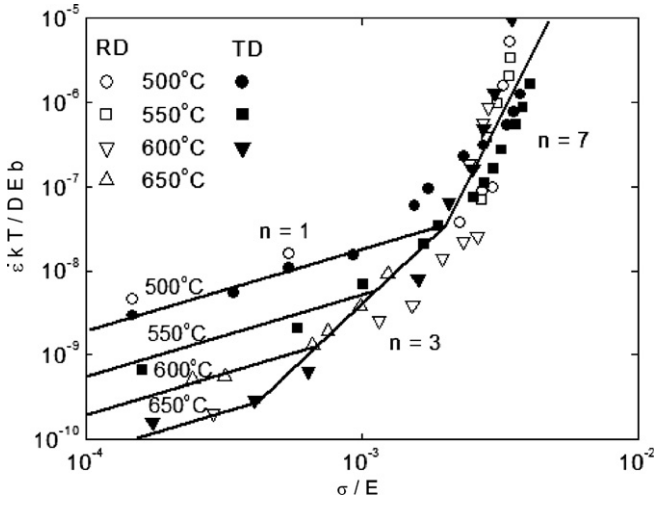

Fig. 6. A normalized plot of the creep data for the Nb-modified Zircaloy showing various deformation regimes [32].

Fig. 7(a) shows a random distribution of dislocations in the viscous glide regime ($n = 3$). This microstructural feature is consistent with the operation of viscous dislocation glide. The sample taken in the $n = 7$ regime shows the presence of sub-boundaries (Fig. 7(b)) which lends support to the operation of dislocation climb controlled creep processes.

Zhou et al. [34] studied a CWSR Zirlo alloy tubing using closed end internal pressurization creep tests. However, unlike most of the creep tests discussed so far, this produces a biaxial stress state (a stress ratio i.e. the ratio of hoop stress to axial stress of ~2). The hoop strain rates were found to be significant compared to the axial creep rates. The normalized hoop strain rates against normalized hoop stresses are plotted in Fig. 8. Here also the Nb-added alloy acts like a Class-A alloy with a clear presence of a $n = 3$ regime.

5. Creep properties of M5 alloy

Recently, M5 (a Zr–Nb–O alloy, see Table 1) alloy has been developed to serve as a high performance cladding

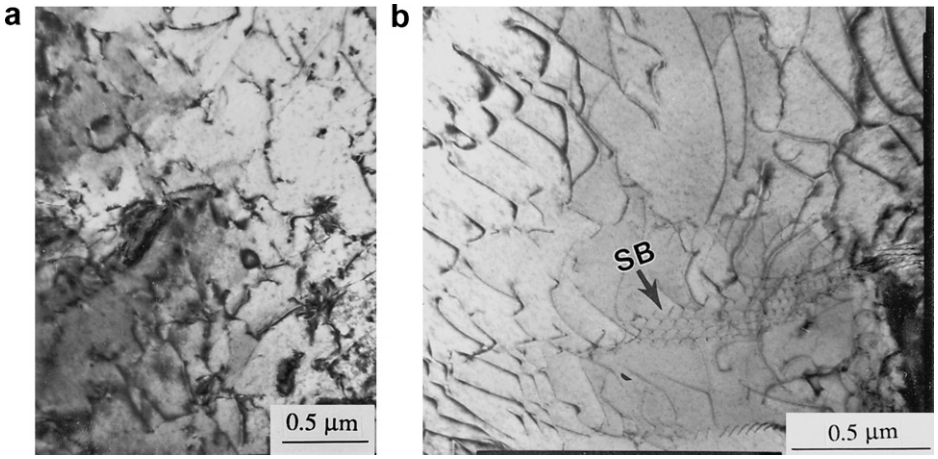

Fig. 7. Representative dislocation features observed in (a) $n = 3$ and (b) $n = 7$ deformation regimes (SB – sub-boundaries) [11].

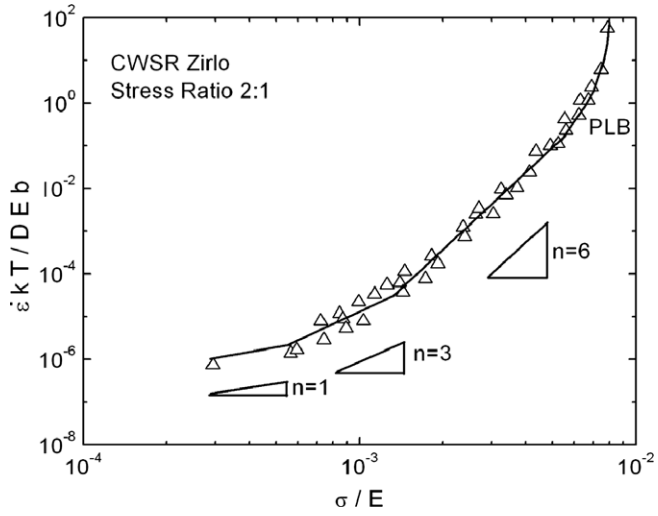

Fig. 8. A plot of normalized hoop strain rates against hoop stresses for CWSR Zirlo tubing [34].

material. Although the composition is similar to those of some Russian alloys, the processing is the key. Very little is known about the creep properties of this alloy. However, recently Brenner et al. [35] have presented a limited amount of data on the creep characteristics of M5 tubing. M5 tubing under two different conditions (one referred to as 'A' experienced thermal cycle only below the monotectoid temperature, and the other one, 'B,' alternatively above and below that temperature during the fabrication) were investigated. Fig. 9 shows a comparison between the creep curves of alloy-A and alloy-B. Alloy-B is much stronger than the alloy-A. However, these two alloys have the similar texture, composition, grain size and shape. Even the stress exponent value was identical (~4). However, they found a difference in the precipitate microstructure. Alloy-A had a more homogeneous β-Nb precipitate structure whereas alloy-B showed heterogeneous distribution of the precipitates. However, through careful TEM study they concluded that there was no greater dislocation density near the precipitates in alloy-B than alloy-A, and thus hardening due to precipitates during creep is not a viable explanation. They found through X-ray spectrometric investigation that the alloy-B contained more Nb (by 0.1 wt%) in α-Zr phase than that of alloy-A. Therefore, the solid solution strengthening may have caused the difference in creep rates between the two alloys. More detailed evaluation of creep data is called for in elucidating the underlying micromechanisms.

6. Creep properties of Zr–Sn–Mo–Nb alloy

Pahutova et al. [36] studied the creep properties of a Zr–3Sn–1Mo–1Nb (by wt%) alloy in a temperature range of 350–550 °C. The prior β-Zr grain size of the alloy was 220 μm. The alloy with dislocated martensitic structure was aged so that a very small volume fraction of β-Zr remained in the microstructure. All the creep data (steady state strain rate and stress) pertaining to this material was normalized with appropriate diffusivity and modulus, as shown in Fig. 10. Unlike the previous data, all data were obtained at high stresses ($>10^{-3}$ E) only. Hence, only two deformation regimes were observed. At lower normalized stress, a stress exponent of 3 was obtained and a stress exponent of 6 at intermediate stress levels implying that the alloy behaves as a Class-A type with viscous glide of dislocations dominating at lower stresses below around 3×10^{-3} E while breakaway from solute locking leading to dislocation-climb controlled creep. At very high stresses ($>10^{-2}$E), it exhibited power law breakdown. It would have been interesting to study creep at lower stress regimes and/or higher temperatures to examine the possibility of grain boundary sliding and Newtonian viscous creep regimes as has previously been observed in Zr–1Nb alloys.

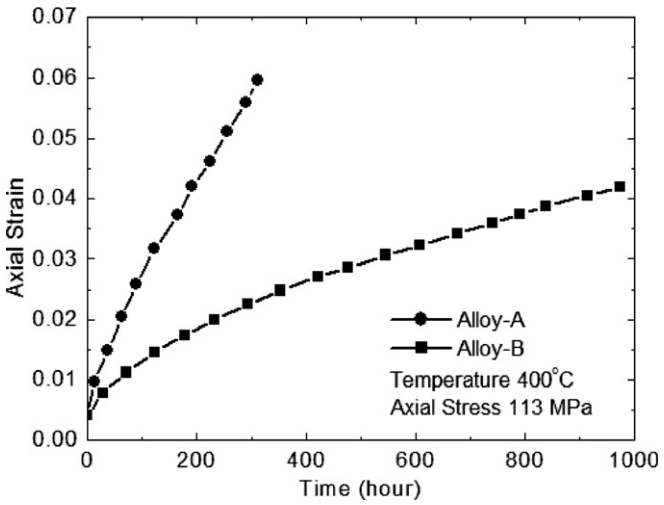

Fig. 9. Creep curves for alloy-A and alloy-B tested at 400 °C and an axial stress of 113 MPa [35].

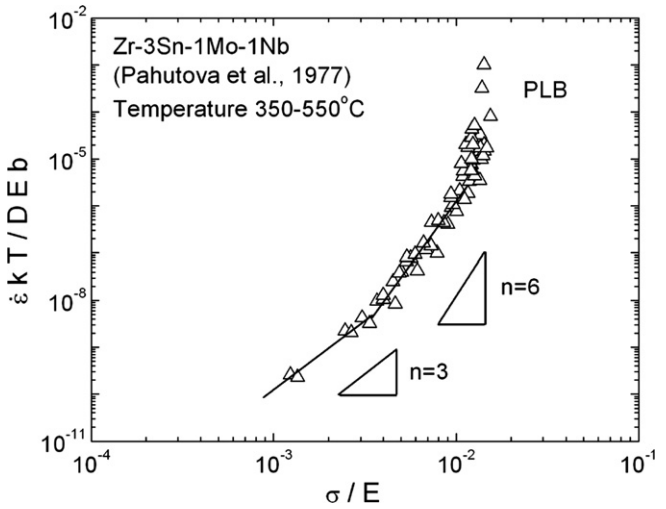

Fig. 10. Normalized steady-state creep rate vs. normalized stress data for a Zr–3Sn–1Mo–1Nb alloy [36].

It is clear that Nb and perhaps Mo form solute atmospheres locking the gliding dislocations.

7. Discussion

In the preceding sections, we have discussed deformation mechanisms in several Nb-containing Zr-based alloys. In Fig. 11, we have shown most data in the form of data trace only from the actual experimental data presented earlier for a clear interpretation. In addition, actual creep data of a recrystallized Zircaloy-4 [37], and a data trend for commercially pure (CP) Zr as compiled by Hayes et al. [5] are also included. Furthermore, only data corresponding to dislocation-based creep mechanisms (grain size independent) are used to construct the figure. Here data from recrystallized alloys under uniaxial creep conditions have only been considered. From this figure, following interesting points can be noted:

(a) The creep strengths of all alloys are more than the commercially pure Zr (which shows typical Class-M creep behavior i.e. dislocation climb controlled behavior).
(b) It appears from the figure that the addition of Nb does not increase the creep resistance after 0.5 wt% or so since the Zr–1Nb data fall almost close to the Zr–0.5Nb data. However, note that we have not dealt with the higher Nb-containing alloys and the statement made previously may not be true for them.
(c) As evident from Fig. 11, the creep data of a recrystallized Zircaloy-4 alloy (average grain size of 15 μm) almost superimpose on the Zr–1Nb or Zr–0.5Nb data. The atomic radius of Sn is only 3% larger than that of Zr whereas the Nb atom is about 9% larger [36]. However, the modulus mismatch will be substantial for Nb compared to Sn with respect to Zr. Therefore, the reason for having similar creep strength in Zircaloy-4 is not readily discernible.
(d) For the alloy Zr–1Sn–1Nb–0.2Fe, the creep strength is much higher than Zr, Zircaloy-4 or Zr–Nb alloys. Hence, the presence of both Sn and Nb is instrumental in augmenting the creep strength through solid solution strengthening and/or particle strengthening.
(e) The strongest alloy is found to be Zr–3Sn–1Mo–1Nb alloy. A higher amount of Sn and the concomitant presence of Nb and Mo (the size mismatch of Mo and Zr atoms is ~13% as well as large modulus mismatch [36]) increased the creep strength of the alloy.
(f) It has been shown that the Nb containing Zr alloys behave as a Class-A solid solution, involving the operation of the viscous dislocation glide mechanism (through the viscous drag exerted by the Nb solute atmospheres formed around the mobile dislocations) yielding a stress exponent of 3. It is likely that moderate atomic size mismatch and large modulus mismatch of Nb in Zr lattice cause a strong interaction between the Nb atoms and dislocations, thus resulting in the creation of solute atmospheres around mobile dislocations in the viscous dislocation glide regime. This deformation regime is not present in Zr or Zircaloys. However, the precise effect of Nb on the viscous glide needs to be further examined.
(g) It is interesting to note that in Zr-based alloys PLB occurs at relatively higher modulus-compensated stresses than usually noted in many metallic systems.

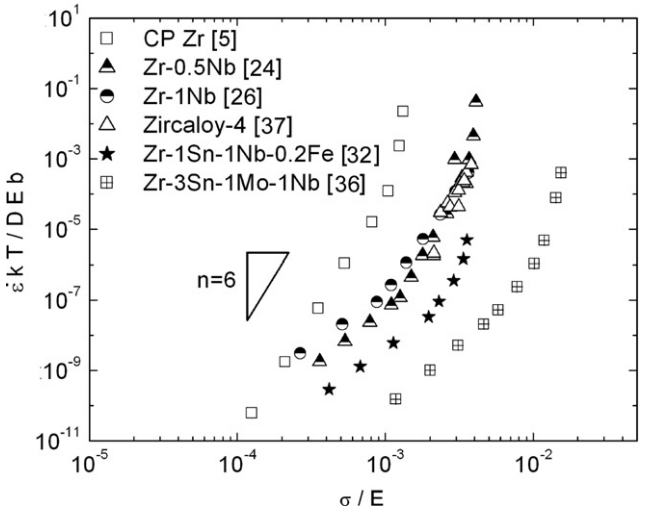

Fig. 11. Comparison of normalized strain rate–stress data for various Zr-based materials.

It is important to remember that Zr alloys have characteristic textures (often dependent on the specific fabrication details [6]), which may lead to anisotropic creep behavior. Thus, textures may influence the creep properties discussed above. As all the reports wherefrom the creep data were collected did not elaborate on the textural characteristics, one should be cautious while making definitive conclusions from Fig. 11. Further, modulus and diffusivity data should be carefully chosen, and the effect of impurities present in the alloys need to be carefully examined.

From the previous discussion on various deformation mechanisms and the possibility of their transitions depending on the test conditions, it is clear that this knowledge is very important in evaluating and predicting the creep performance of cladding in reactors. One needs to understand that the presence of such transitional mechanisms can lead to non-conservative estimates of the creep rates as a result of blind extrapolation of higher stress data to lower stresses corresponding to in-service conditions.

8. Conclusions

Creep along with high temperature deformation data are analyzed from different studies on Nb-modified Zr alloys. Only the creep data of Zr alloys containing less than 1.2 wt% Nb are analyzed in detail. The data were also com-

pared with the creep data of Zr and Zircaloy-4. It is found that higher Nb addition may not necessarily enhance the creep resistance. But under certain conditions of temperatures and stresses, the Nb-containing alloys may behave as a Class-A type alloy due to the solute-drag dislocation glide, which is not found in Zr or Zircaloys. Through this, the importance of transitional creep mechanisms is further emphasized in the estimation of reactor cladding life. More creep studies on the advanced alloys like Zirlo and M5 would be needed to fully understand their creep characteristics.

Acknowledgments

We gratefully acknowledge the financial support of the US National Science Foundation through grants DMR0101309 and DMR0412583, and the DOE-NEER grant DE-FG07-04ID14611. We also wish to convey our sincere appreciation to the reviewers for constructive suggestions.

References

[1] K.L. Murty, Appl. Mech. Rev. 46 (5) (1993) 194.
[2] J.T.A. Roberts, Structural Materials in Nuclear Power Systems, Plenum, NY, 1981.
[3] F.H. FroesMaterials Science and Technology – a Comprehensive Treatment, vol. 8, VCH, Weinheim, Germany, 1996, p. 399.
[4] D.G. Franklin, G.E. Lucas, A.L. Bement, Creep of Zirconium Alloys in Nuclear Reactors, STP 815, ASTM, Philadelphia, PA, 1983.
[5] T.A. Hayes, M.E. Kassner, R.S. Rosen, Metall. Mater. Trans. 33A (2) (2002) 337.
[6] K.L. Murty, I. Charit, Prog. Nucl. Energ. 48 (2006) 325.
[7] R. Krishnan, M.K. Asundi, in: S. Ranganathan, V.S. Arunachalam, R.W. Cahn (Eds.), Alloy Design, Indian Academy of Sciences, 1981, p. 139.
[8] A.V. Nikulina, Met. Sci. Heat Treat. 45 (7–8) (2003) 287.
[9] I.T. Bethune, C.D. Williams, J. Nucl. Mater. 29 (1969) 129.
[10] H. Okamoto, J. Phase Equilib. 13 (5) (1992) 577.
[11] M. Canay, C.A. Donon, D. Arias, J. Nucl. Mater. 280 (2000) 365.
[12] J. Ravi, High Temperature Creep of Nb-Modified Zircaloy, M.S. Thesis, NC State University, 1991.
[13] O.D. Sherby, P.M. Burke, Prog. Mater. Sci. 13 (1968) 323.
[14] T.G. Langdon, in: Proceedings of Dislocations and Real Properties of Materials, Inst. of Materials, London, UK, 1985, p. 221.
[15] K.L. Murty, Scripta Met. 7 (1973) 899.
[16] K.L. Murty, Mater. Sci. Eng. 14 (1974) 169.
[17] J. Weertman, J. Appl. Phys. 28 (10) (1957) 1185.
[18] K.L. Murty, in: J.C. Earthman, F.A. Mohamed (Eds.), Proceedings of 7th International Conference on Creep and Fracture of Engineering Materials and Structures, August 1997, TMS, p. 69.
[19] P. Yavari, T.G. Langdon, Acta Metall. 30 (12) (1982) 2181.
[20] G.M. Hood, J. Nucl. Mater. 139 (1986) 179.
[21] N. Matsuura, G.M. Hood, H. Zou, J. Nucl. Mater. 238 (1996) 260.
[22] G.M. Hood, J. Nucl. Mater. 159 (1988) 149.
[23] V.S. Lyashenko, V.N. Bykov, L.V. Pavlinov, Phys. Met. Metallogr. 8 (3) (1959) 40.
[24] M. Pahutova, J. Cadek, V. Cerny, J. Nucl. Mater. 61 (1976) 285.
[25] W.R. Thorpe, I.O. Smith, J. Nucl. Mater. 75 (1978) 209.
[26] M.I. Alymov, E.N. Pirogov, L.L. Artyaukhina, Atom. Energ. 62 (6) (1987) 387.
[27] V.P. Voeikov, A.M. Kapteltsev, D.A. Ozertskii, V.Y. Tonkov, Vopr. At. Nauk. Tekh., Ser. At. Materialoved. 17 (1984) 24.
[28] M.I. Alymov, E.N. Pirogov, L.L. Artyukhina, O.V. Komarov, Atom. Energ. 65 (3) (1987) 791.
[29] E.N. Pirogov, O.V. Komarov, M.I. Alymov, Atom. Energ. 66 (4) (1989) 271.
[30] E.N. Pirogov, M.I. Alymov, L.L. Artyukhina, Atom. Energ. 65 (4) (1988) 293.
[31] G.P. Tiwari, B.D. Sharma, V.S. Raghunathan, R.V. Patil, J. Nucl. Mater. 46 (1973) 35.
[32] K.L. Murty, G. Dentel, J. Britt, Mater. Sci. Eng. A 410&411 (2005) 28.
[33] K.L. Murty, J. Ravi, Nucl. Eng. Des. 156 (3) (1995) 359.
[34] Y. Zhou, B. Devarajan, K.L. Murty, Nucl. Eng. Des. 228 (1–3) (2004) 3.
[35] R. Brenner, J.L. Bechade, O. Castelnau, B. Bacroix, J. Nucl. Mater. 305 (2002) 175.
[36] M. Pahutova, K. Kuchanova, J. Cadek, Mater. Sci. Eng. 27 (1977) 239.
[37] W.L. Daugherty, Biaxial Creep of Zircaloy: Texture and Temperature Effects, PhD Thesis, NC State University, 1988.